

Feedback Control of Functional Electrical Stimulation for 2D Arm Reaching Movements

Reza Sharif Razavian, Borna Ghannadi, Naser Mehrabi, Mark Charlet, and John McPhee

Abstract—Functional electrical stimulation (FES) can be used as a neuroprosthesis in which muscles are stimulated by electrical pulses to compensate for the loss of voluntary movement control. Modulating the stimulation intensities to reliably generate movements is a challenging control problem. This paper introduces a feedback controller for a multi-muscle FES system to control hand movements in a two-dimensional (table-top) task space. This feedback controller is based on a recent human motor control model, which uses muscle synergies to simplify its calculations and improve the performance. This synergy-based controller employs direct relations between the muscle synergies and the produced hand force, thereby allowing for the real-time calculation of six muscle stimulation levels required to reach an arbitrary target. The experimental results show that this control scheme can perform arbitrary point-to-point reaching tasks in the two-dimensional task space in real-time, with an average of ~ 2 cm final hand position error from the specified targets. The success of this prototype demonstrates the potential of the proposed method for the feedback control of functional tasks with FES.

Index Terms—Functional electrical stimulation (FES), muscle synergies, feedback control, task space control, biomechanics.

I. INTRODUCTION

Functional electrical stimulation (FES) is the process of applying external electrical pulses to skeletal muscles or to their attached nerves, in order to generate force in the muscle and perform actions. The electric pulses are usually in the form of a high-frequency pulse train, where the frequency, amplitude and pulse width can all be modulated to change the muscle force.

Artificial stimulation of muscles has long been an intriguing idea to produce functional movements in individuals with motor impairments. Furthermore, the application of FES to rehabilitation programs has shown improved recovery of post-stroke patients, even in severe and chronic cases [1], [2]. Despite the attractiveness of the FES systems, however, there are basic challenges that prevent them from being widely used.

The biggest challenge is associated with the complexity of the human musculoskeletal system; it is a redundant, non-linear and noisy system with significant uncertainties. The actuators in the human body are the muscles, many of which are co-activated by the nervous system to produce a certain motion. We do not know how the nervous system calculates

the required muscle activities. Thus, we have yet to mimic the same process to produce naturally-looking motions with FES.

Many methods are presented in the literature for the control of FES devices. Finite state controllers [3]–[5] switch between different *states* based on the measurements of the system, but during each state the controller is essentially feed-forward. Another important trend is to use an artificial neural network to generate the FES control signals [6]–[8]. PID [9], [10] and sliding-mode controllers [11], [12] have also been used for the control of FES systems. Optimal control methods (e.g. non-linear model predictive controllers [13]–[15]) have been proposed as well.

These previous FES controllers (except for the finite state controllers [3], [4]) were limited to simple motions: either the single-joint knee or elbow flexion/extension [5]–[7], [11]–[14]) or the two degree of freedom (DoF) motion of ankle [8]. The control of more complex multi-joint systems were only tested in computer simulations [9], [10]. The generalizability of these controllers to multi-DoF and multi-muscle systems has not been reported.

Controlling upper extremity movements with FES is a challenging control problem, mostly because of the large number of DoFs and involved muscles. A single-muscle controller for a one-dimensional (1D) reaching task has been developed in [16], [17]. The control of elbow extensor to facilitate reaching movements was reported in [18], [19]. The only multi-muscle controllers for the upper extremity are [20]–[22]. Isometric hand force production was studied in [20], while [22] presented the estimation of FES-produced joint torques during a prescribed 3D movement. Finally a feed-forward motion controller for reaching tasks was developed in [21].

All the developed FES controllers for the upper extremity [16], [18]–[22] have taken a joint space approach, in which the effect of muscle activities on the joint torques are calculated, and then inverse kinematics/dynamics is used to convert the information from the task space (hand position, which is the controlled variable) to the joint space (for which the models are developed). This added complexity can be removed by developing the formulation in the task space, and considering the effect of muscles on the task space forces, rather than the joint torques.

In this paper, we employ a biologically-inspired human motor control model [23], [24] to develop a real-time feedback controller for FES. The advantage of this model is in its task space representation, which liberates the controller from the joint-space complexities. Furthermore, muscle synergies are used as a biologically-plausible method [25]–[27] to further simplify the relationship between task variables (i.e. hand position) and muscle activities. The goal of the developed

R. S. Razavian is with the Department of Systems Design Engineering, University of Waterloo, Waterloo, Ontario, Canada. e-mail: rsharifr@uwaterloo.ca

B. Ghannadi is with MapleSoft Inc., Waterloo, Canada

N. Mehrabi is with the Department of Mechanical Engineering, University of Washington

Mark Charlet is with the Department of Engineering Physics, Laval University

J. McPhee is with the Department of Systems Design Engineering, University of Waterloo

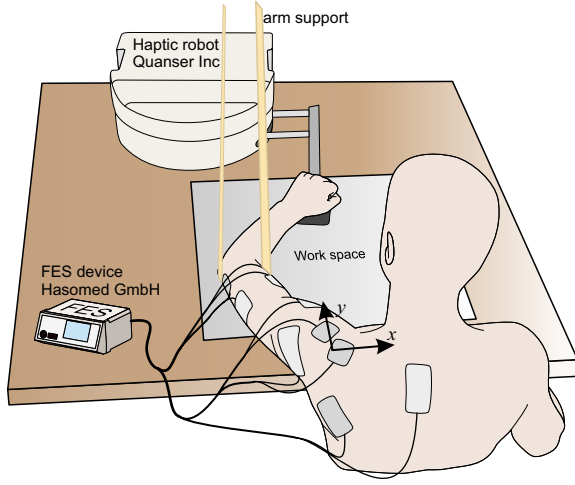


Fig. 1. The experimental setup for testing the motor control framework as the feedback controller for an FES system. The passive electrodes are indicated with darker shades.

controller is to activated major upper extremity muscles and drive the arm to arbitrary targets in a two-dimensional (2D tabletop) workspace.

II. METHODS

A. The experimental setup

The experimental setup is shown in Fig. 1. The stimulation device is RehaStim V.1 with Science Mode (Hasomed GmbH, Germany), which stimulates six muscles of the left arm (anterior and posterior deltoid, biceps and triceps brachii, pectoralis major, and the intermediate region of trapezius). The electrical pulses are delivered to the muscles via the electrode pads (5×13 cm) placed on the skin and over the muscle motor points as suggested by [28]. The passive electrodes (5×5 cm) were placed away from the motor points. Minor location adjustments were allowed to reduce discomfort. The stimulation frequency and current are fixed at 33 Hz (to ensure smooth force production [29]) and 20 mA, respectively, and the stimulation pulse width is modulated using a computer running Matlab/Simulink.

The goal in this setup is to use the motor control framework as the FES controller, to control the position of the hand, and drive it to any arbitrary target in a 2D (table-top) space. For this purpose, the hand position and the forces applied to the hand are measured using a 2D haptic robot (Quanser Inc. Canada). The robot can be programmed to be locked in place (for isometric trials), or move while applying resistance (during motion trials). The subject sits upright in front of the robot. A wrist brace is used to restrict the wrist's degrees of freedom, and also firmly connect the hand to the robot's end-effector. To reduce the arm-table friction and keep the arm in the horizontal plane, the arm is suspended using a sling. Since the arm always remains elevated by the sling at a certain height, the effective number of the arm's degrees of freedom is reduced to two; thus, only the (x, y) position of the hand is sufficient to describe the posture. For this argument to be valid, it is assumed that the torso movement is negligible, and

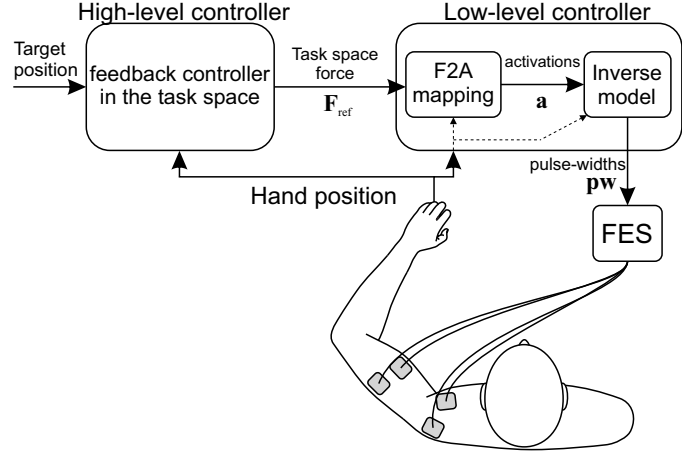


Fig. 2. The overview of the motor control model as the FES feedback controller

the scapula motion is linked to the shoulder elevation/flexion angles (through *scapulohumeral rhythm*).

This FES controller was tested on left arms of three healthy subjects (21, 28 and 31 years old, all male and right-handed). To minimize the subjects' voluntary actions, they were asked to relax, and no information about the intended action was visible to them.

B. FES controller architecture

The feedback FES controller is the real-time implementation of a synergy-based motor control model [23], [24]. The advantage of this motor control model is in its task space representation, which simplifies the calculations and allows for efficient control of the movements in the task space. The task space in this context is defined as a 2D Cartesian space, specified by the (x, y) position of the hand. Alternatively, for example, if the objective were to control the elbow flexion angle only, the task space would be a 1D space defined by elbow angle (the hand position would be irrelevant in this case).

The schematic of the motor control model as the FES feedback controller is shown in Fig. 2. This model has a hierarchical structure. The high-level controller is a feedback controller that compares the actual hand position with the specified target, and defines the direction in which the hand has to move. The high-level controller in this implementation is a PID controller; its input is the position error in the task space, and it defines a 2D reference force, \mathbf{F}_{ref} , which is required to reach to the specified target.

This force command should be fulfilled by activating the muscles. Thus, the role of the low-level controller is to translate the task space force command to muscle activations and consequently to stimulation pulse width (pw). This force-to-activation (F2A) mapping uses *muscle synergies* to calculate the muscle activations from the reference force. A muscle synergy in this context is defined as the co-activation of a number of muscles with predetermined relative ratios (specified by a column vector $\mathbf{S} = [a_1, a_2, \dots, a_6]^T$). The basics of the F2A mapping is briefly explained here.

TABLE I
THE PARAMETERS USED IN THE EXPERIMENTS

Parameter	value
PID coefficients	$K_P = 150 \text{ (Nm}^{-1}\text{)}$
	$K_d = 30 \text{ (Nsm}^{-1}\text{)}$
	$K_i = 30 \text{ (Ns}^{-1}\text{m}^{-1}\text{)}$
Cost function weightings	$w_1 = 1000 \text{ (N}^{-2}\text{)}$
	$w_2 = 1 \times 10^{-6} \text{ (}\mu\text{s}^{-1}\text{)}$
	$w_3 = 1 \text{ (N}^{-2}\text{)}$

In a given posture, defined by the hand's (x, y) position in the task space, the activation of a single synergy, S , results in a certain isometric hand force (vectors B in Fig. 3). Each of these force vectors that are produced by individual synergies can be considered as a *basis vector* for the task space; the collection of all the vectors is then a *basis set* for the task space. The basis set and the synergy matrix are expressed as:

$$\mathbf{B}_{2 \times k} = [B_1, B_2, \dots, B_k] \quad (1)$$

$$\mathbf{S}_{6 \times k} = [S_1, S_2, \dots, S_k] \quad (2)$$

where k is the number of muscle synergies.

The known basis vectors can be used to solve for the muscle activations in real-time, instead of the time-consuming optimization process (e.g. in [20], [21]). The force vector command \mathbf{F}_{ref} can be decomposed into the basis set to calculate the coefficient of each basis vector (Fig. 3). This problem is equivalent to solve for the vector C in the equation:

$$\mathbf{F}_{\text{ref}} = \mathbf{B}_{2 \times k} C_{k \times 1} \quad (3)$$

Then, the synergies are combined using the calculated coefficients as

$$\mathbf{a}_{6 \times 1} = \mathbf{S}_{6 \times k} C_{k \times 1} \quad (4)$$

to obtain the muscle activations that produce the reference force. The schematic and block diagram of this process is shown in Fig. 3.

C. Implementation of the FES controller

To implement this motor control framework as the FES controller, subject-specific *models* of the stimulated muscles are needed. Specifically, to calculate the basis vectors, one should have an estimate of the forces generated by individual muscles. Because of the task-dependent architecture of the motor control framework, it is only required to identify a mapping that transforms a muscle's stimulation intensity (pw) to the task space force vector. This feature is an important advantage of the proposed motor control model as no explicit information about the kinematics of the body (e.g. segment lengths and joint angles) and the joint moments is necessary.

1) *Identifying pulse-width-to-force mappings*: The subject-specific muscle models used in this work are static input-output functions that estimate the 2D task space force for each muscle from the stimulation intensity and the hand position:

$$\mathbf{F}_{\text{est}} : \mathbb{R}^3 \rightarrow \mathbb{R}^2 \\ (pw, x, y) \mapsto (F_x, F_y) \quad (5)$$

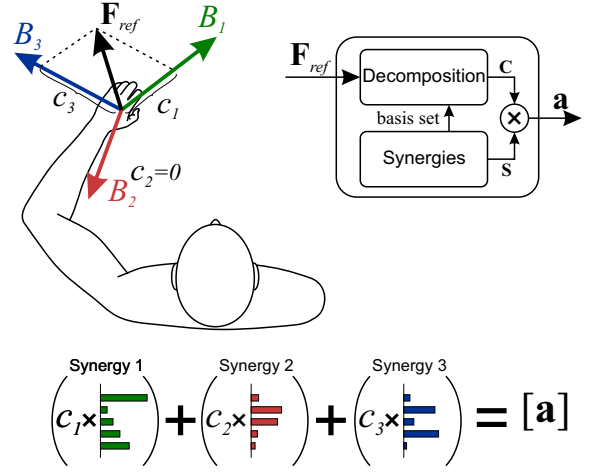


Fig. 3. The schematic of the F2A mapping. Each synergy produces a certain force in the task space, which can be considered as a basis vector. An arbitrary reference force, \mathbf{F}_{ref} , can be decomposed into this basis set, to calculate the coefficient of each synergy, c_i . Combining the synergies with the corresponding coefficients gives the vector of muscle activations that produces the reference force.

To obtain the muscle mappings of this form for each muscle, a subject's individual muscles are isometrically stimulated (the robot is locked in place) one by one with the profiles similar to those shown in Fig. 4a, and the hand force/position is measured by the robot. The profiles in Fig. 4a are subject-specific, where the base pulse width values are the onset of feeling the stimulations on the skin (no force is produced at this level of stimulation), and the maximum values are the thresholds where the stimulations become uncomfortable for the subject. These thresholds are obtained prior to testing via manual modulation of stimulations for each muscle. Using these patterns, only one muscle is active in each instant of time; therefore, the measured force contains the contribution of a single muscle only. The stimulations are repeated at multiple positions in the considered workspace (Fig. 4b) to account for the posture-dependence of the produced forces.

The mapping in (5) is constructed by training two separate mappings: the first one is trained to estimate the direction of the hand force as a function of posture, and the second one estimates the hand force magnitude as a function of posture and stimulation pulse width. The reason for the separation of the force direction from its magnitude is to ensure that the direction of the estimated force remains the same for all intensity levels (ideally this direction should only depend on the geometry of the musculoskeletal system). Unless indwelling or nerve cuff electrodes are used, the assumption of constant force direction may not hold, as higher stimulation intensities with transcutaneous electrodes may excite the neighbouring muscle fibres and alter the direction of the hand force. Nonetheless, the motor control model relies on this assumption; thus, the force direction mapping is trained despite the changing stimulation intensity, and is only a function of the posture. In addition, these feed-forward mappings need only be approximate, as the high-level feedback controller can compensate the modelling error.

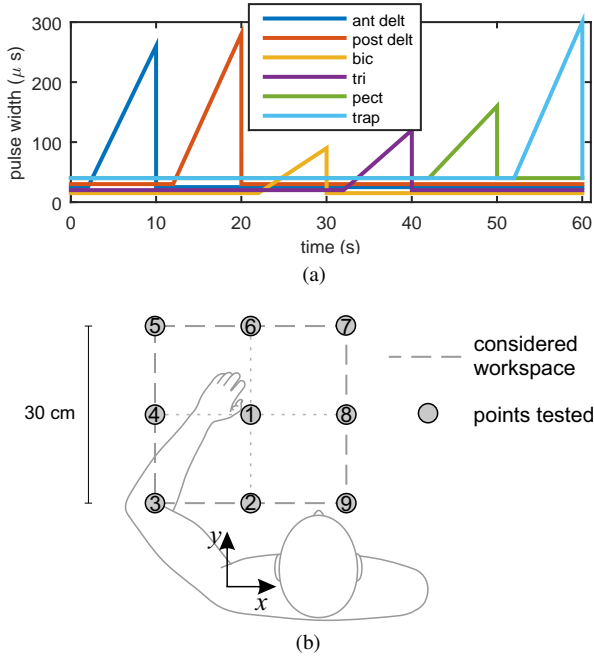


Fig. 4. (a) The stimulation profiles used to train the muscle mappings (these profiles belong to subject #1). For each muscle, the maximum pulse width is the threshold where the stimulation becomes uncomfortable for the subject, and the base value is the onset of feeling the stimulations on the skin (no force is produced at this level of stimulation). (b) The workspace and the points at which the stimulation profiles are applied. The thresholds are the same for all the tested points. The numbers inside the circles indicate the *posture IDs* that are referred to in Fig. 9

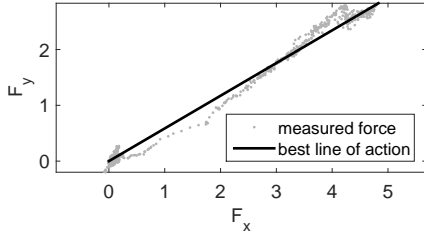


Fig. 5. An example for the best line of action (pectoralis major muscle in the centre of the workspace for subject #1). The dots represent the measured force as the pulse-width increases.

a) *The direction mapping*: The direction mapping is trained using the *best line of action* of the measured hand forces at various postures. This line of action is obtained by fitting a line (zero y-intercept) to the measured force (as seen in Fig. 5). Next, the unit vector, $\hat{\mathbf{u}}_F$, representing this direction is found, and second-order polynomial surfaces ($\mathcal{P}(x, y)$) are used to fit its u_x and u_y components as functions of the hand position.

$$\hat{\mathbf{u}}_F = \begin{bmatrix} u_x \\ u_y \end{bmatrix} = \begin{bmatrix} \mathcal{P}_1(x, y) \\ \mathcal{P}_2(x, y) \end{bmatrix} \quad (6)$$

Fig. 6 shows the estimated force directions of subject #1's stimulated muscles in the 2D task space. In these plots, the origin of the coordinate system is at the left shoulder, x is lateral with the positive direction pointing to the right, and y is forward (see Fig. 4b). The goodness of the polynomial

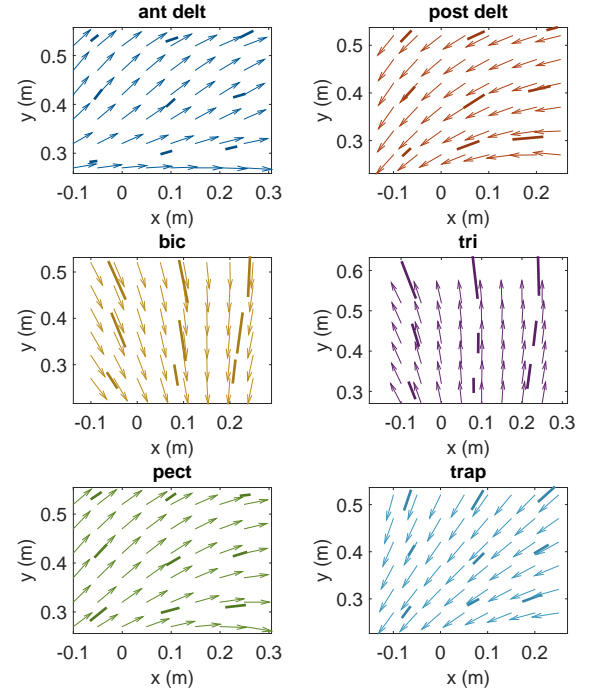


Fig. 6. The trained mappings for the direction of the force in the entire workspace. The best line of action of the measured data are shown with thick lines, and the arrows show the direction of the force estimated by the mapping. The force measurements are shown with $1\text{N} = 0.005\text{m}$ scale in this plot.

fit (adjusted R-squared) for the direction mapping is given in Table II.

b) *The amplitude mapping*: The amplitude mapping contains two fitted functions. The estimation of the posture-dependent maximum force is obtained using a second-order polynomial surface, which is fitted to the maximum of the measured force amplitudes (at maximum pulse-width, $|\mathbf{F}(pw_{max})|$) in various postures. This mapping gives the maximum hand force production capacity of the muscle as a function of posture as:

$$F_{max} = \mathcal{P}_3(x, y) \quad (7)$$

Fig. 7 shows the estimated maximum task space forces of subject #1's muscles. The goodness of the fit for F_{max} (adjusted R-squared) is given in Table II.

The last function is used to estimate the *muscle activation*, a . Muscle activation in this context is defined as the linear scaling of the maximum force, between 0 and 1:

$$a(pw) := \frac{|\mathbf{F}(pw)|}{|\mathbf{F}(pw_{max})|} \quad (8)$$

The muscle activation is a non-linear function of the stimulation pulse width, which is modelled using a sigmoid function. Sigmoid is chosen because stimulated muscle forces tend to be S-shaped, and because sigmoid functions are easily invertible. During the experiments, it was observed that the activation- pw relation is not significantly affected by the

TABLE II
THE GOODNESS OF FIT (ADJUSTED R-SQUARED) FOR THE TRAINED MUSCLE MAPPINGS.

Muscle	Subject #1				Subject #2				Subject #3			
	u_x	u_y	F_{max}	a	u_x	u_y	F_{max}	a	u_x	u_y	F_{max}	a
Anterior deltoid	0.202	0.126	0.227	0.900	-0.097	0.0780	0.798	0.778	0.300	0.375	0.817	0.876
Posterior deltoid	0.949	0.945	0.940	0.909	0.258	0.457	0.716	0.635	0.880	0.413	0.807	0.901
Biceps	0.987	0.784	0.921	0.906	0.968	0.926	-0.489	0.923	0.746	0.393	0.525	0.906
Triceps	0.995	0.886	0.828	0.965	0.738	0.070	0.955	0.782	0.722	0.389	0.891	0.759
Pectoralis Major	0.633	0.727	0.884	0.918	0.043	0.625	0.266	0.746	0.014	0.080	0.079	0.411
Trapezius	0.929	0.918	0.639	0.950	0.900	0.926	0.266	0.746	0.558	0.137	0.512	0.757

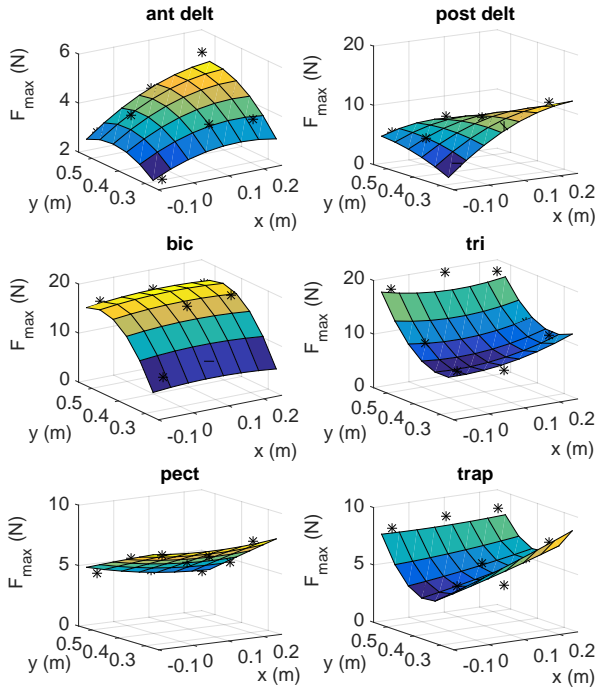


Fig. 7. The fitted polynomial surfaces to estimate the maximum capacity of the muscles as functions of posture. The measured data are shown with black asterisks. These results belong to subject #1.

posture (only the maximum force changes by posture, see Fig. 8). Therefore, the following sigmoid function, \mathcal{S} , with four parameters c_i is trained using the collection of the data obtained at all the postures.

$$a = \mathcal{S}(pw) = c_1 + \frac{c_2 - c_1}{1 + 10^{(c_3 - pw)c_4}} \quad (9)$$

The trained amplitude mappings (the combination of the activation and F_{max} mappings) for the stimulated muscles are shown in Fig. 9. The quality of the sigmoid fit (adjusted R-squared) is also given in Table II for all the muscles.

Finally, the three subject-specific functions are combined to obtain the subject-specific *posture-dependent pulse-width-to-force mappings* for individual muscles:

$$\mathbf{F}_{est}^i(pw, x, y) = \hat{\mathbf{u}}_F^i(x, y) F_{max}^i(x, y) a^i(pw) \quad (10)$$

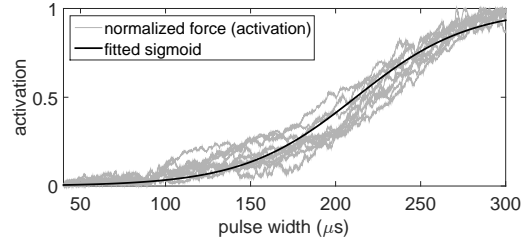


Fig. 8. The sigmoid function fitted to the measured data collected at 9 different positions in the workspace (the example data belongs to subject #1's pectoralis major muscle)

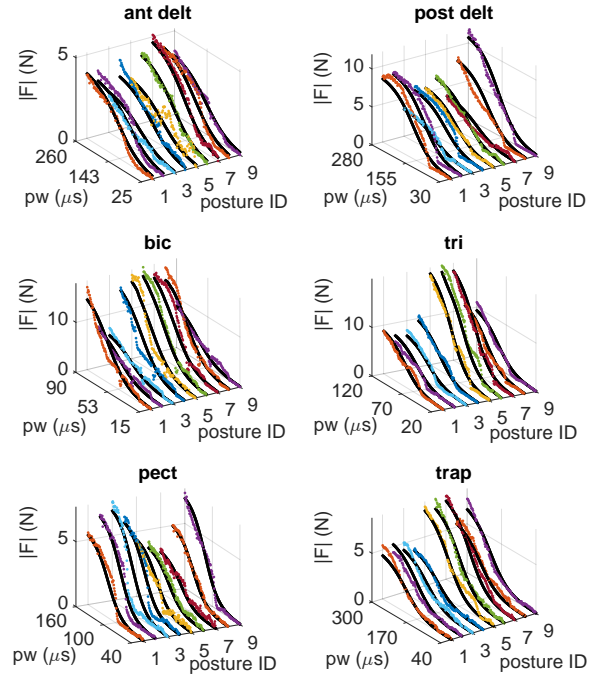


Fig. 9. Subject #1's estimated force amplitudes as functions of stimulation pulse width in various postures (identified by *position ID* in the plots). The amplitude estimations (black lines) are compared against the measured force amplitudes (coloured dots).

where $\hat{\mathbf{u}}_F^i$, F_{max}^i and a^i are the functions that estimate the force unit vector, maximum muscle capacity, and activation level of the i^{th} muscle, respectively. The first two functions are

the polynomial surfaces, and the last one is a sigmoid function. Using these functions, the basis vector corresponding to the synergy $S = [a_1, a_2, \dots, a_6]^T$ can be estimated as:

$$B(x, y) = \sum_{i=1}^6 \hat{\mathbf{u}}_F^i(x, y) F_{max}^i(x, y) a_i \quad (11)$$

where the index i represents the i^{th} muscle.

Defining muscle activation is important in the synergy framework, as its relationship with muscle force is linear—a feature that is necessary for the superposition principle that is the core of the synergy framework. Stimulation pulse width, unfortunately, does not exhibit such a relationship. Once the required muscle activations are calculated through the processes in the F2A mapping, an *inverse mapping* is required to calculate the needed stimulation pulse widths. The inverse mapping $pw = S^{-1}(a)$ can be easily obtained by taking the inverse of the sigmoid function in (9) as:

$$pw = S^{-1}(a) = c_3 - \frac{1}{c_4} \log \left(\frac{c_2 - a}{a - c_1} \right) \quad (12)$$

2) *Obtaining the synergies*: The muscle synergies in this framework need to have an important feature: their basis vectors must span the task space in such a way that any force vector can be a linear combination of the basis vectors with *positive coefficients* (muscles are pull-only elements). This requirement implies that: 1) at least three synergies are required to control the motion in the 2D task space, and 2) their basis vectors cannot all be in one half-plane. Furthermore, the structure of the synergies may affect the performance of the control loop. As a result, proper identification of the synergies is an important step in this motor control model.

Three methods are studied to obtain the synergies; one is a heuristic method, and the other two include factorization matrices that contain optimal muscle activation data.

In the heuristic method, the muscles with similar functions are grouped together and stimulated with fixed relative activation levels. In this context, a muscle's function is defined as the direction of the hand force it produces. Therefore, the synergy 1 includes anterior deltoid and pectoralis major muscles; synergy 2 includes posterior deltoid and trapezius muscles; synergy 3 includes biceps brachii; finally, synergy 4 includes triceps brachii.

The direction of forces produced by each synergy varies with posture, but in rough terms, synergy 1 moves the hand medially, synergy 2 moves the hand laterally, synergy 3 retracts the hand, and synergy 4 pushes the hand away from the body. As an example, subject #1's heuristic synergies and the associated basis vectors are visualized in Fig. 10a.

The basis vectors that the heuristic synergies produce can successfully span the task space (see Fig. 10b). However, it should be noted that this property may not necessarily hold in general. For instance, muscles may change function drastically across larger or more complex task spaces. More importantly, the inclusion of more muscles makes it harder to identify such synergies. For example, the trapezius muscle is placed in the synergy 2 alongside the posterior deltoid, but its function is to retract the scapula and consequently move the hand laterally

and back, which is neither the same as the posterior deltoid nor biceps brachii. Therefore, considering more systematic methods to obtain useful synergies is highly beneficial.

A non-negative matrix factorization (NNMF) algorithm [30] is used to calculate the synergies more systematically. To start the process, a large number of optimization problems are solved. In a particular posture, the best set of muscle activations that results in a target hand force is found. For this purpose, the muscle mappings are used to find the estimates for the hand forces. The target hand forces, \mathbf{F}_{tgt} , in the optimizations are 15 equally-spread vectors (with 24° differences) at a given point in the horizontal plane. The optimization algorithm tries to minimize the objective function J :

$$\mathbf{a}_{6 \times 1}^* = \arg \min_{0 < a_i < 1} \{J\} \quad (13)$$

$$J = w_1 \left\| \left(\sum_{i=1}^6 \mathbf{F}_{est}^i \right) - \mathbf{F}_{tgt} \right\|^2 + w_2 \sum_{i=1}^6 pw_i + w_3 \sum_{i=1}^6 |F_{est}^i|^2 \quad (14)$$

where the index i represents the i^{th} muscle, and w 's are weighting factors to balance and non-dimensionalize the terms (values given in Table I). In this cost function, the first term is the penalty function forcing the estimated total hand force (generated by all the active muscles) to match the target force, the second term penalizes high stimulation intensities, and the last one has the effect of sharing the load among similar-function muscles.

The optimal activations that produce the 15 target forces can be gathered in the matrix:

$$\mathbf{A}_{6 \times 15} = [\mathbf{a}_1^*, \mathbf{a}_2^*, \dots, \mathbf{a}_{15}^*] \quad (15)$$

The usual practice of using NNMF is applied to this data matrix to obtain the synergy matrix \mathbf{S} and the coefficient matrix \mathbf{C} as:

$$\mathbf{A}_{6 \times 15} \simeq \mathbf{S}_{6 \times k} \mathbf{C}_{k \times 15} \quad (16)$$

where k is the number of synergies (represented by the columns of \mathbf{S}).

This process is repeated at p different postures to obtain the posture-dependent synergies with posture-dependent bases. Fig. 10c shows the results when $p = 64$ (an 8×8 grid in the task space). As a rule of thumb we found that a grid point at every 4 cm in the workspace provides sufficiently smooth transitions of the synergies between postures.

Alternatively, the optimal activation matrices in all the p postures can be stacked in a larger matrix and then fed to the NNMF algorithm to get the posture-dependent synergies with shared bases:

$$\mathbf{A}_{6p \times 15} = \begin{bmatrix} \mathbf{A}_{6 \times 15}^1 \\ \mathbf{A}_{6 \times 15}^2 \\ \vdots \\ \mathbf{A}_{6 \times 15}^p \end{bmatrix} = \begin{bmatrix} \mathbf{S}_{6 \times k}^1 \\ \mathbf{S}_{6 \times k}^2 \\ \vdots \\ \mathbf{S}_{6 \times k}^p \end{bmatrix} \mathbf{C}_{k \times 15} \quad (17)$$

This *concatenated* NNMF method (CNNMF) [31] has the advantage of giving synergies that are readily consistent across

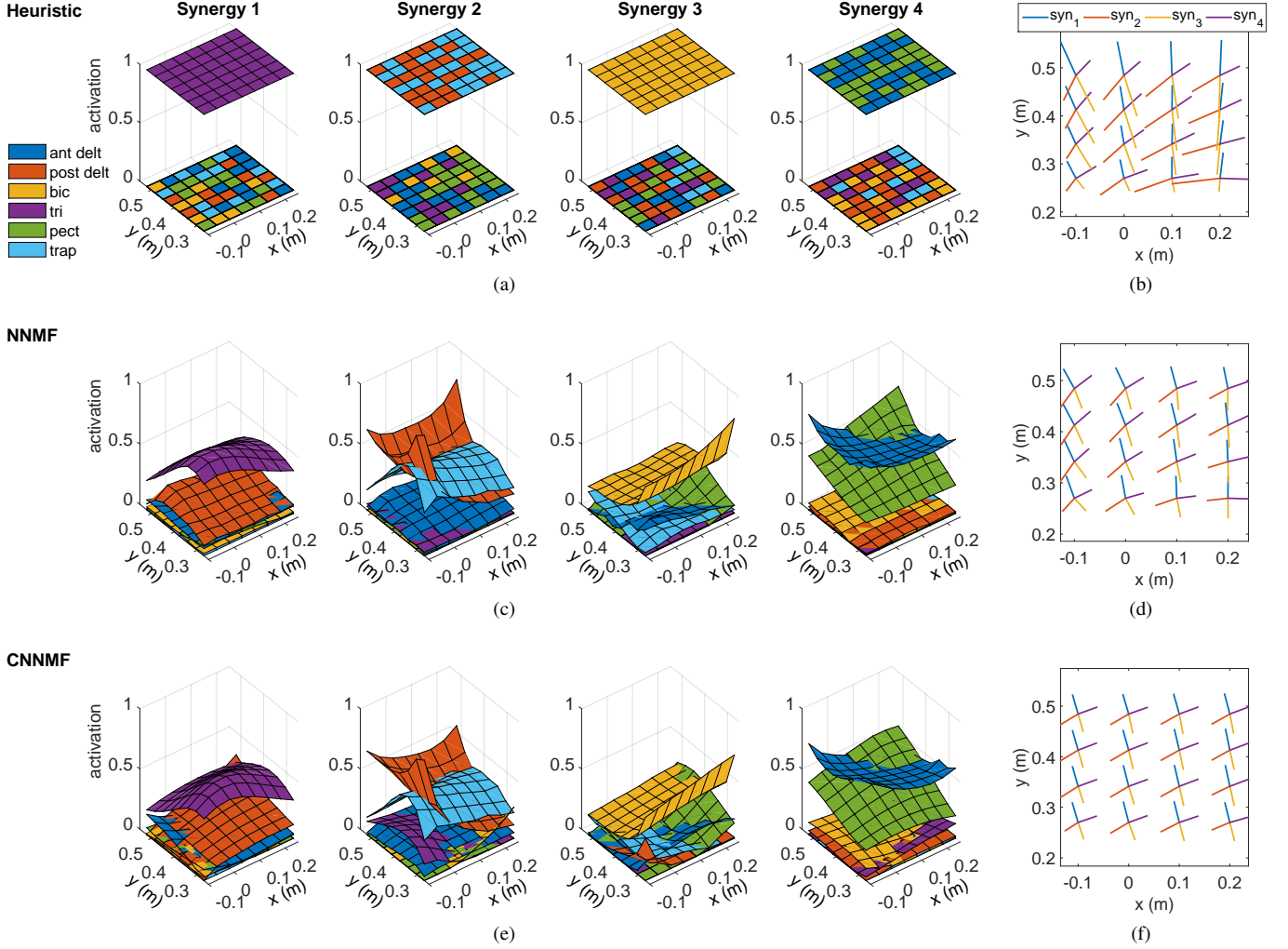


Fig. 10. Subject #1's synergies (panels a, c, and d) and the corresponding basis vectors in the 2D task space (panels b, d, and f) obtained from the three methods. **Top row:** the heuristic method (fixed synergies, changing bases). **Middle row:** the normal NNMF method (changing synergies, changing bases). **Bottom row:** CNNMF method (changing synergies, fixed bases). Each surface in these plots shows how the activation of a muscle in a synergy changes across various postures in the task space. The checkerboard patterns in the heuristic synergies mean that multiple surfaces are on top of each other. The basis vectors on the right are the estimated task space forces from the combined muscle activities in each synergy (obtained using the identified muscle mappings). These basis vectors are drawn with 0.01 m/N scale.

posture (i.e. the transition of synergies from one posture to a neighbouring one is always smooth). This is a feature that is hard to achieve using the normal NNMF method because of the many local minima in its solution space. Furthermore, as can be observed in equation (17), the coefficient matrix is shared between all postures, implying that the basis vectors are approximately posture-invariant—another feature that helps with the calculations in the F2A mapping. Fig. 10e shows the synergies obtained from the CNNMF method and the corresponding basis vectors.

To get the estimate of the total hand force that each synergy produces (i.e. the basis vectors in Figures 10b, 10d and 10f), the synergies obtained from any of the three methods were fed to the muscle mappings. Therefore, one should note that the bases are estimates themselves, rather than the exactly measured response of the muscles.

D. The experiment procedure

Three healthy subjects participated in the experiments. The experiments were approved by the Office of Research Ethics at the University of Waterloo, and participants gave informed consent to take part in the experiment. Since the participants retained full voluntary control over their muscles, they were instructed to relax as much as possible and avoid performing any voluntary movement.

In the first set of tests, isometric trials were performed. In these tests, the robot was locked in four different locations in the task space, and the F2A algorithm estimated the stimulation pulse widths that would generate reference isometric hand forces (5-N forces in 6 different directions). Then the muscles were stimulated with the calculated pulse widths, and the actual hand force was measured. These trials were meant to assess the combined performance of two components of the framework: the first component is the muscle mapping, and the second one is the F2A. The existence of inaccuracies

in each part results in error in the force produced.

Next, the motor control model was used as the feedback motion controller for the FES system. Random point-to-point movements (not visible to the subjects) were chosen as the reference trajectories, to reduce the chance of memorizing the trajectory and voluntarily following it. The subjects were also asked to relax as much as possible to further reduce the chance of voluntary actions.

During the real-time control of the movement, the hand position is measured by the robot, which is used to interpolate between the previously calculated synergy matrices and basis sets. The interpolation gives the synergies and bases at the current posture. This information is then used in the F2A mapping to get the muscle activations, which are finally converted by the inverse mapping to pulse-width commands that are sent to the FES device.

All subjects did separate sets of tests using the three different synergy methods. The exception is subject #2, who did not test with NNMF synergies.

III. RESULTS

Fig. 11 shows the reference (big circles) and the resulting hand forces (small dots that are color coded) in isometric trials of subjects #1, #2 and #3. The three methods compared are: the heuristic synergies (denoted as *heuristic* in the plots), the factorized synergies with posture-dependent bases (denoted by NNMF), and the factorized synergies with shared bases (denoted by CNNMF). No NNMF data was recorded for subject #2. Four synergies are used in all the methods for consistency. Although there is error between the targets and the actual hand forces, this error is mostly compensated by the high-level feedback controller in the motion trials. Similar performances are observed in the resulting data for subject #1 and #3, while higher relative errors are observed for subject #2.

The closed-loop FES control performance is shown in Fig. 12, where the reference motions were sequences of randomly placed target points. The maximum hand velocity experienced in the reference trajectory is approximately 25 cm/s. The resulting movements from the different synergy extraction methods are shown for the three subjects. The tracking error is also visualized in Fig. 13. The average distance of the hand from the specified targets at the end of the reaching movements is approximately 2 cm with all three methods for subject #1, 3 cm for subject #2 and 1 cm for subject #3. The histogram of hand position errors for the entire motion is also shown in Fig. 13. Because of the high-velocity portions of the reference trajectories at the transition points, the total error has a larger mean and standard deviation value.

IV. DISCUSSION

It is debatable whether muscle synergies are truly the building blocks of muscle activities. Both arguments favouring (e.g. [32], [33]) and rebutting (e.g. [34]) the muscle synergy theory exist (for a review see [35]). Nonetheless, muscle activations do show synergistic patterns in normal human movements. Therefore, the proposed synergy-based FES controller, which

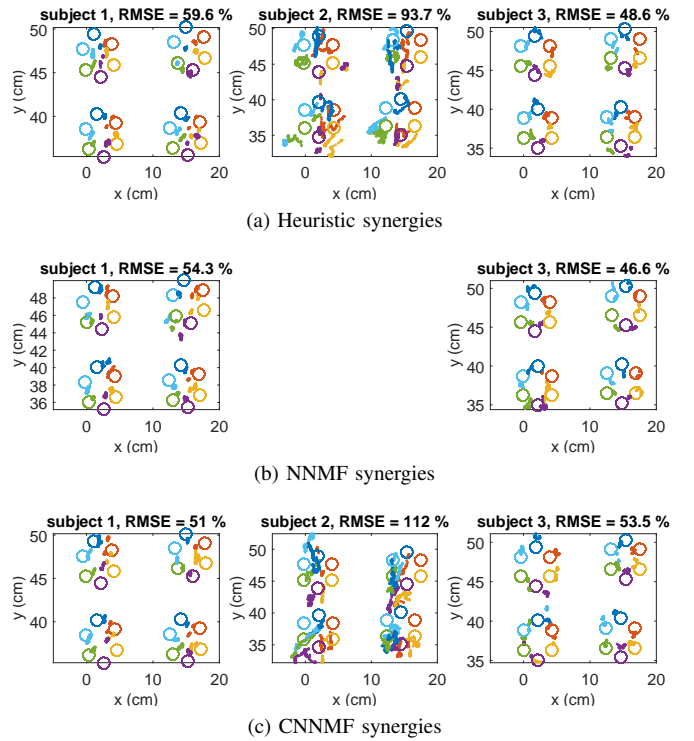


Fig. 11. The results from the isometric force production trials performed on three subjects, using (a) heuristic, (b) NNMF, and (c) CNNMF synergies. The relative root-mean-squared of error (RMSE) is provided. In these tests, the reference hand forces are six equally-spaced vectors of amplitudes 5 N (forces drawn with 0.005 m/N scale). Subject #2 did not test with NNMF synergies.

results in the synergistic co-activation of the muscles, has the potential to mimic natural control of movements better than single-muscle controllers.

The motor controller presented in this paper takes advantage of the known muscle actions in the task space, to reduce the computational time and improve control performance. The experimental results showed that the choice of the synergy extraction method has a small effect on the tracking performance of the feedback controller. The tracking performance seems to be more affected by the quality of the muscle mappings (i.e. goodness of fit in Table II) than by the choice of the synergies. It is worth noting that the synergies extracted from simulated optimal muscle activities (e.g. the NNMF and CNNMF methods) are shown in [36] to have a similar structure as the ones obtained from real electromyographic data of healthy individuals. This may justify the extra effort needed to obtain synergies with the factorization methods, as opposed to the heuristic one.

The relatively high force production error in the isometric trials (50-60% for subjects #1 and #3 and appropriately 100% for subject #2 in Fig. 11) may have many causes, including the inaccuracies in the muscle mappings (which give the basis vectors), inaccuracies in the vector decomposition (which relies on linearity assumption), inaccuracies in the activation-to-pulse width mapping (to calculate the required pulse-widths), and altered electrode/muscle conditions (including skin impedance and muscle fatigue). Statistical analysis shows that the choice of the synergy method has no significant effect on the results of either the isometric trials (one-way ANOVA results:

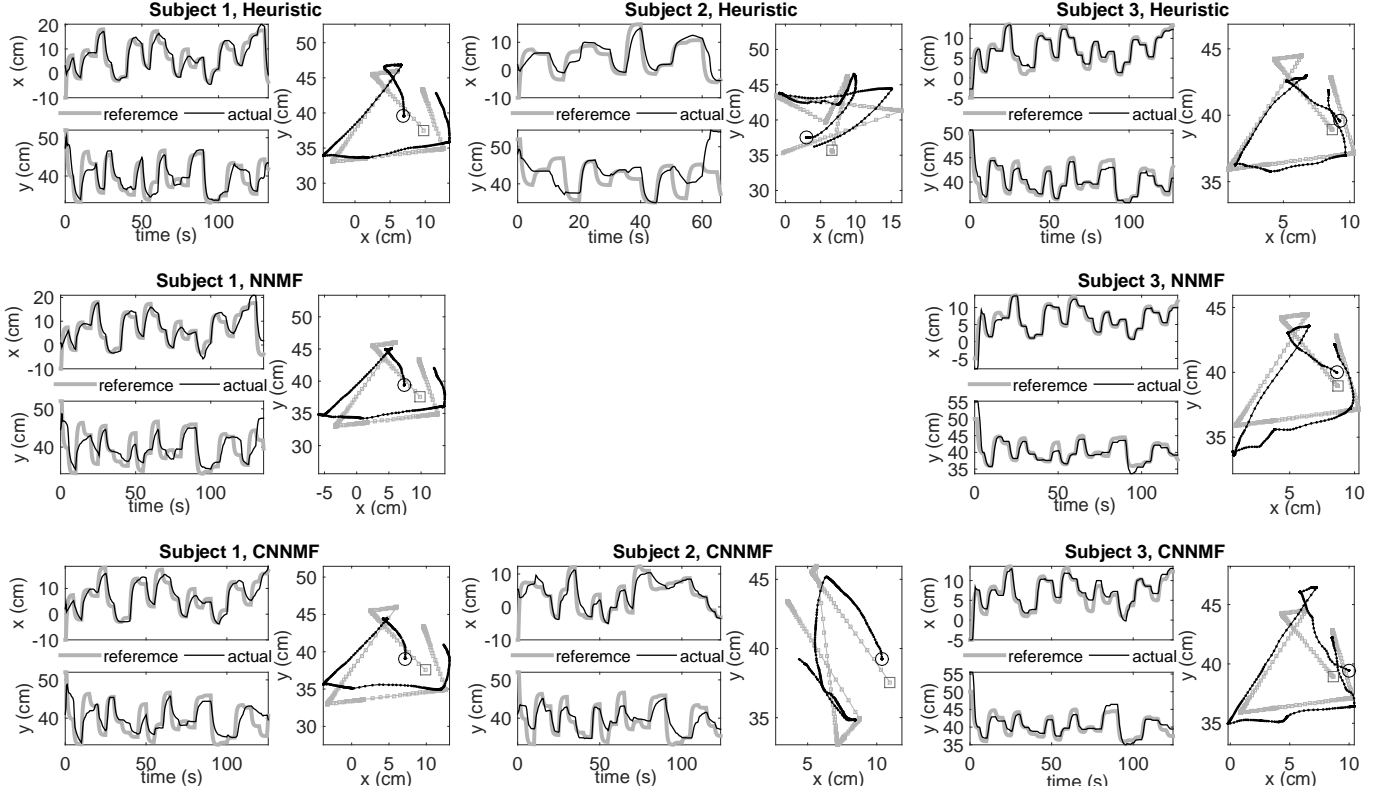


Fig. 12. The feedback control performance resulting from the three synergy calculation methods for subjects #1, #2 and #3. The plots on the left for each subject show the reference trajectories (thick grey lines) and the actual movements (thin black lines) of the hand in the 2D task space. The plots on the right show 80-110 s of the randomly generated paths (grey) and the produced motion (black). The starting position is indicated by large circles and squares. Subject #2's reference paths were different from those of the other two subjects. NNMF synergy results for subject #2 were not recorded.

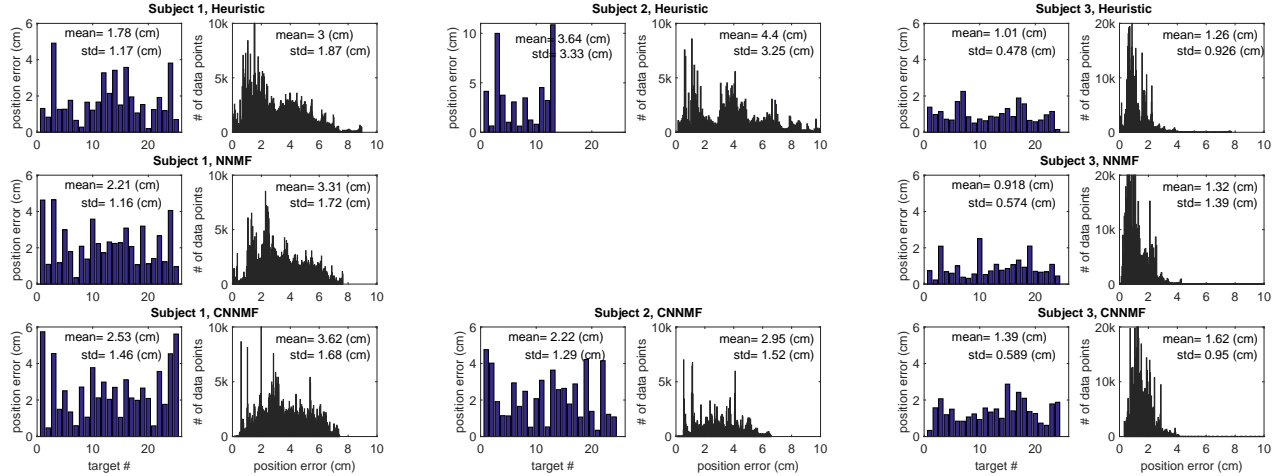


Fig. 13. Feedback controller tracking error. For each subject, the left column shows the position error between the target and the actual hand position at the end of each reaching movement, and the right column shows the histogram of the error in the entire duration of the movements. The histogram plots show the number of sample times with the amount of error indicated by the horizontal axis.

$p = 0.096$, $p = 0.116$, and $p = 0.272$ for subjects #1, #2, and #3, respectively) or the motion trials ($p = 0.118$, $p = 0.69$, for subject #1 and #2). The only statistically significant difference has been observed in subject #3's tracking error, where the heuristic method is different from the other two methods

($p < 0.05$). Our observations suggest that the quality of the fitted surfaces during muscle mapping identification has a stronger effect on the tracking performance of the controller. Subject #2's inferior control performance could be attributed to poor muscle mapping quality (note the lower goodness of fit

in Table II). Furthermore, the changes in muscle/skin condition (e.g., skin conductance, electrode wear, sweat) could also contribute to the error. To compensate for these uncertainties, an on-line method can be used to re-train the muscle mappings based on the inputs and the measurements. The development of such on-line methods, however, is beyond the scope of this paper.

To improve the proposed controller performance, it is also possible to include the system dynamics in the calculations. The hand and robot dynamics cause inaccuracies in the F2A estimation of muscle activations. Furthermore, all the information stored in the controller (in the form of the synergies and the basis set) belongs to isometric conditions. As a result, the controller performance further degrades when the velocities are large. To account for the velocity-dependent accelerations and inertial effects, the arm's equations of motion, as well as its model parameters are needed (as described in [37]). Unfortunately, obtaining such information is time consuming, which will increase the proposed method's preparation time (about 10-15 minutes in our tests). In a clinical setting where therapy time is limited, one should weight the benefit of the improved control performance over the cost of the time spent on parameter identification.

The controller was tested on three healthy subjects. However, there is no restriction in the controller architecture that prevents the method from being applied to impaired individuals. As long as the muscles are strong enough and respond to the stimulations, the controller can be applied. However, there are potential challenges with a clinical population that may impact the controller performance. For example, stroke patients may suffer from spastic muscles, joint contracture, and day-to-day changes in neuromuscular responses, which may adversely affect the FES controller performance. These issues are essentially *disturbances* to the systems, which can be accommodated by the proposed *feedback* control structure.

A prominent problem with all transcutaneous FES systems is the inconsistent response of the muscles to the stimulations between subjects, and in a single subject between different sessions. The presented method is no exception, and needs to be calibrated for each subject and therapy session. The strength of the method, on the other hand, is its inherent subject-specificity.

The presented FES controller was used to reach to targets on a 2D tabletop surface. The motor control framework used as the controller has the ability to be generalized to higher dimensions. For instance, the same motor control framework has been used to simulate reaching to targets in 3D space [37]. Therefore, the FES controller can be extended without significant modification to handle the 3D motions in activities of daily living, which are also more attractive for rehabilitation purposes.

V. CONCLUSION

The application of a synergy-based motor control model to the feedback controller of functional electrical stimulation devices was presented. As an advantage, this control method only required information in a task space, which disentangles the control task from many of the complexities of the

musculoskeletal system, allowing for fast feedback control of the motions. As a result, the proposed FES controller is the first of its kind that can be used to generate and control arbitrary movements in a 2D task space. The experimental results on three different subjects showed that the synergy-based motor control model could be used to produce reaching movement with approximately 1-3 cm accuracy as measured at the endpoint.

ACKNOWLEDGMENT

The authors wish to thank the Natural Sciences and Engineering Research Council of Canada (NSERC) and the Canada Research Chairs program for funding support of this study.

REFERENCES

- [1] N. M. Kapadia, M. K. Nagai, V. Zivanovic, J. Bernstein, J. Woodhouse, P. Rumney, and M. R. Popovic, "Functional Electrical Stimulation Therapy for Recovery of Reaching and Grasping in Severe Chronic Pediatric Stroke Patients," *Journal of Child Neurology*, vol. 29, pp. 493–499, apr 2014.
- [2] T. A. Thrasher, V. Zivanovic, W. McIlroy, and M. R. Popovic, "Rehabilitation of Reaching and Grasping Function in Severe Hemiplegic Patients Using Functional Electrical Stimulation Therapy," *Neurorehabilitation and Neural Repair*, vol. 22, no. 6, pp. 706–14, 2008.
- [3] T. C. Bulea, R. Kobetic, M. L. Audu, J. R. Schnellenberger, and R. J. Triolo, "Finite state control of a variable impedance hybrid neuroprosthesis for locomotion after paralysis," *IEEE Transactions on Neural Systems and Rehabilitation Engineering*, vol. 21, no. 1, pp. 141–151, 2013.
- [4] M. J. Bauman, T. M. Bruns, J. B. Wagenaar, R. A. Gaunt, and D. J. Weber, "Online feedback control of functional electrical stimulation using dorsal root ganglia recordings," *Conference proceedings : ... Annual International Conference of the IEEE Engineering in Medicine and Biology Society. IEEE Engineering in Medicine and Biology Society. Conference*, vol. 2011, pp. 7246–9, jan 2011.
- [5] P. E. Crago, W. D. Memberg, M. K. Usey, M. W. Keith, R. F. Kirsch, G. J. Chapman, M. A. Katorgi, and E. J. Perreault, "An elbow extension neuroprosthesis for individuals with tetraplegia," *IEEE Transactions on Rehabilitation Engineering*, vol. 6, no. 1, pp. 1–6, 1998.
- [6] J. J. Abbas and H. J. Chizeck, "Neural network control of functional neuromuscular stimulation systems: computer simulation studies," *IEEE Transactions on Biomedical Engineering*, vol. 42, pp. 1117–27, nov 1995.
- [7] F. Previdi, "Identification of black-box nonlinear models for lower limb movement control using functional electrical stimulation," *Control Engineering Practice*, vol. 10, no. 1, pp. 91–99, 2002.
- [8] H. Park and D. M. Durand, "Motion control of musculoskeletal systems with redundancy," *Biological Cybernetics*, vol. 99, pp. 503–16, dec 2008.
- [9] K. M. Jagodnik, D. Blana, A. J. van den Bogert, and R. F. Kirsch, "An optimized proportional-derivative controller for the human upper extremity with gravity," *Journal of Biomechanics*, vol. 48, no. 13, pp. 3701–3709, 2015.
- [10] K. M. Jagodnik and A. J. van den Bogert, "Optimization and evaluation of a proportional derivative controller for planar arm movement," *Journal of Biomechanics*, vol. 43, pp. 1086–1091, apr 2010.
- [11] A. Ajoudani and A. Erfanian, "A Neuro-Sliding Mode Control With Adaptive Modeling of Uncertainty for Control of Movement in Paralyzed Limbs Using Functional Electrical Stimulation," *IEEE Transactions on Biomedical Engineering*, vol. 56, no. 7, pp. 1771–1780, 2009.
- [12] C. L. Lynch and M. R. Popovic, "A comparison of closed-loop control algorithms for regulating electrically stimulated knee movements in individuals with spinal cord injury," *IEEE transactions on neural systems and rehabilitation engineering : a publication of the IEEE Engineering in Medicine and Biology Society*, vol. 20, pp. 539–48, jul 2012.
- [13] N. Kirsch, N. Alibej, and N. Sharma, "Nonlinear model predictive control of functional electrical stimulation," *Control Engineering Practice*, vol. 58, pp. 319–331, jan 2017.

- [14] N. Kirsch, N. Alibej, and N. Sharma, "Nonlinear Model Predictive Control of Functional Electrical Stimulation," in *Volume 2: Diagnostics and Detection; Drilling; Dynamics and Control of Wind Energy Systems; Energy Harvesting; Estimation and Identification; Flexible and Smart Structure Control; Fuels Cells/Energy Storage; Human Robot Interaction; HVAC Building Energy M*, p. V002T27A005, ASME, oct 2015.
- [15] N. Mehrabi, S. Tajeddin, N. L. Azad, and J. McPhee, "Application of Newton/GMRES Method to Nonlinear Model Predictive Control of Functional Electrical Stimulation," in *The 3rd International Conference on Control, Dynamic Systems, and Robotics (CDSR'16)*, no. 121, (Ottawa, Canada), pp. 3–7, may 2016.
- [16] C. T. Freeman, A.-M. Hughes, J. H. Burridge, P. H. Chappell, P. L. Lewin, and E. Rogers, "A model of the upper extremity using FES for stroke rehabilitation," *Journal of Biomechanical Engineering*, vol. 131, p. 031011, mar 2009.
- [17] C. Zhuang, J. C. Marquez, H. E. Qu, X. He, N. Lan, I. S. Member, H. E. Qu, X. He, I. S. Member, and N. Lan, "A neuromuscular electrical stimulation strategy based on muscle synergy for stroke rehabilitation," *2015 7th International IEEE/EMBS Conference on Neural Engineering (NER)*, no. July 2015, pp. 816–819, 2015.
- [18] D. Popovic and M. Popovic, "Tuning of a nonanalytical hierarchical control system for reaching with FES," *IEEE Transactions on Biomedical Engineering*, vol. 45, no. 2, pp. 203–212, 1998.
- [19] M. Popovic and D. Popovic, "Cloning biological synergies improves control of elbow neuroprostheses: Simulating natural control of the extremities using inductive learning," *IEEE Engineering in Medicine and Biology Magazine*, vol. 20, no. 1, pp. 74–81, 2001.
- [20] E. M. Scheerer, Y.-W. Liao, E. J. Perreault, M. C. Tresch, W. D. Memberg, R. F. Kirsch, and K. M. Lynch, "Multi-Muscle FES Force Control of the Human Arm for Arbitrary Goals," *IEEE Transactions on Neural Systems and Rehabilitation Engineering*, vol. 22, pp. 654–663, may 2014.
- [21] E. M. Scheerer, Y.-W. Liao, E. J. Perreault, M. C. Tresch, W. D. Memberg, R. F. Kirsch, and K. M. Lynch, "Evaluation of a Semi-Parametric Model for High-Dimensional FES Control," *2015 7th International IEEE/EMBS Conference on Neural Engineering (NER)*, pp. 304–307, 2015.
- [22] E. M. Scheerer, Y.-W. Liao, E. J. Perreault, M. Tresch, W. D. Memberg, R. F. Kirsch, and K. M. Lynch, "Semiparametric Identification of Human Arm Dynamics for Flexible Control of a Functional Electrical Stimulation Neuroprosthesis," *IEEE Transactions on Neural Systems and Rehabilitation Engineering*, vol. 24, no. April, pp. 1–1, 2016.
- [23] R. Sharif Razavian, *A Human Motor Control Framework based on Muscle Synergies*. Phd thesis, University of Waterloo, 2017.
- [24] R. Sharif Razavian, N. Mehrabi, and J. McPhee, "A model-based approach to predict muscle synergies using optimization: application to feedback control," *Frontiers in Computational Neuroscience*, vol. 9, no. October, pp. 1–13, 2015.
- [25] A. D'Avella, A. Portone, L. Fernandez, and F. Lacquaniti, "Control of fast-reaching movements by muscle synergy combinations," *The Journal of neuroscience : the official journal of the Society for Neuroscience*, vol. 26, pp. 7791–810, jul 2006.
- [26] A. D'Avella, L. Fernandez, A. Portone, and F. Lacquaniti, "Modulation of phasic and tonic muscle synergies with reaching direction and speed," *Journal of neurophysiology*, vol. 100, pp. 1433–54, sep 2008.
- [27] A. de Rugy, G. E. Loeb, and T. J. Carroll, "Are muscle synergies useful for neural control?," *Frontiers in Computational Neuroscience*, vol. 7, no. March, pp. 1–13, 2013.
- [28] M. Behringer, A. Franz, M. McCourt, and J. Mester, "Motor point map of upper body muscles," *European Journal of Applied Physiology*, vol. 114, no. 8, pp. 1605–1617, 2014.
- [29] C. L. Lynch and M. R. Popovic, "Functional Electrical Stimulation," *IEEE Control Systems Magazine*, vol. 28, pp. 40–50, apr 2008.
- [30] D. D. Lee and H. S. Seung, "Algorithms for non-negative matrix factorization," *Advances in Neural Information Processing Systems*, vol. 13, no. 1, pp. 556–562, 2001.
- [31] M. Sharif Shourijeh, T. E. Flaxman, and D. L. Benoit, "An approach for improving repeatability and reliability of non-negative matrix factorization for muscle synergy analysis," *Journal of Electromyography and Kinesiology*, vol. 26, pp. 36–43, feb 2016.
- [32] H. Hirai, H. Pham, Y. Ariga, K. Uno, and F. Miyazaki, "Motor Control Based on the Muscle Synergy Hypothesis," in *Cognitive Neuroscience Robotics A: Synthetic Approaches to Human Understanding* (M. Kasaki, H. Ishiguro, M. Asada, M. Osaka, and T. Fujikado, eds.), pp. 25–50, Tokyo: Springer Japan, 2016.
- [33] E. Bizzi, V. C. K. Cheung, A. D'Avella, P. Saltiel, and M. C. Tresch, "Combining modules for movement," *Brain Research Reviews*, vol. 57, pp. 125–33, jan 2008.
- [34] J. J. Kutch, A. D. Kuo, A. M. Bloch, and W. Z. Rymer, "Endpoint Force Fluctuations Reveal Flexible Rather Than Synergistic Patterns of Muscle Cooperation," *Journal of Neurophysiology*, vol. 100, no. 5, pp. 2455–2471, 2008.
- [35] M. C. Tresch and A. Jarc, "The case for and against muscle synergies," *Current Opinion in Neurobiology*, vol. 19, no. 6, pp. 601–607, 2009.
- [36] K. M. Steele, M. C. Tresch, and E. J. Perreault, "The number and choice of muscles impact the results of muscle synergy analyses," *Frontiers in computational neuroscience*, vol. 7, no. August, p. 105, 2013.
- [37] R. Sharif Razavian and J. McPhee, "A motor control framework for the fast control of a 3D musculoskeletal arm motion using muscle synergy," in *The 4th Joint International Conference on Multibody System Dynamics*, (Montral, Canada), 2016.